

# Seismic Electric Signals and $1/f$ “noise” in natural time

P. A. Varotsos,<sup>1,2,\*</sup> N. V. Sarlis,<sup>1</sup> and E. S. Skordas<sup>1,2</sup>

<sup>1</sup>*Solid State Section, Physics Department, University of Athens,  
Panepistimiopolis, Zografos 157 84, Athens, Greece*

<sup>2</sup>*Solid Earth Physics Institute, Physics Department,  
University of Athens, Panepistimiopolis, Zografos 157 84, Athens, Greece*

By making use of the concept of natural time, a simple model is proposed which exhibits the  $1/f^a$  behavior with  $a$  close to unity. The properties of the model are compared to those of the Seismic Electric Signals (SES) activities that have been found to obey the ubiquitous  $1/f^a$  behavior with  $a \approx 1$ . This comparison, which is made by using the most recent SES data, reveals certain similarities, but the following important difference is found: The model suggests that the entropy  $S_-$  under time reversal becomes larger compared to the entropy  $S$  in forward time, thus disagreeing with the experimental SES results which show that  $S$  may be either smaller or larger than  $S_-$ . This might be due to the fact that SES activities exhibit *critical* dynamics, while the model cannot capture all the characteristics of such dynamics.

PACS numbers: 05.40.-a, 05.45.Tp, 91.30.Dk, 89.75.-k

## I. INTRODUCTION

Among the different features that characterize complex physical systems, the most ubiquitous is the presence of  $1/f^a$  noise in fluctuating physical variables[1]. This means that the Fourier power spectrum  $S(f)$  of fluctuations scales with frequency  $f$  as  $S(f) \sim 1/f^a$ . The power-law behavior often persists over several orders of magnitude with cutoffs present at both high and low frequencies. Typical values of the exponent  $a$  approximately range between 0.8 and 4 (e.g., see Ref.[2] and references therein), but in a loose terminology all these systems are said to exhibit  $1/f$  “noise”. Such a “noise” is found in a large variety of systems, e.g., condensed matter systems(e.g. [3]), freeway traffic[4, 5, 6], granular flow[7], DNA sequence[8], heartbeat[9], ionic current fluctuations in membrane channels[10], river discharge[11], the number of stocks traded daily[12], chaotic quantum systems[13, 14, 15, 16], the light of quasars[17], human cognition[18] and coordination[19], burst errors in communication systems[20], electrical measurements[21], the electric noise in carbon nanotubes[22] and in nanoparticle films[23], the occurrence of earthquakes[24] etc. In some of these systems, the exponent  $a$  was reported to be very close to 1, but good quality data supporting such a value exist in a few of them[3]. As a first example we refer to the voltage fluctuations when current flows through a resistor[25]. As a second example we mention the case of Seismic Electric Signals (SES) activities which are transient low frequency ( $\leq 1$ Hz) signals observed before earthquakes [26, 27, 28, 29, 30, 31, 32, 33, 34], since they are emitted when the stress in the focal region reaches a *critical* value before the failure[35, 36]. These electric signals, for strong earthquakes with magnitude 6.5 or larger, are also accompanied by detectable magnetic

field variations[37, 38, 39]. Actually, the analysis of the original time series of the SES activities have been shown to obey a  $1/f$ -behavior[40, 41].

The  $1/f^a$  behavior has been well understood on the basis of dynamic scaling observed at *equilibrium* critical points where the power-law correlations in time stem from the infinite-range correlations in space (see Ref.[2] and references therein). Most of the observations mentioned above, however, refer to *nonequilibrium* phenomena for which -despite some challenging theoretical attempts[42, 43, 44, 45]- possible *generic* mechanisms leading to scale invariant fluctuations have not yet been identified. In other words, despite its ubiquity, there is no yet universal explanation about the phenomenon of the  $1/f^a$  behavior. Opinions have been expressed (e.g., see Ref.[13]) that it does not arise as a consequence of particular physical interactions, but it is a generic manifestation of complex systems.

It has been recently shown[40, 46, 47, 48, 49, 50, 51, 52, 53, 54, 55, 56, 57] that novel dynamic features hidden behind the time series of complex systems can emerge if we analyze them in terms of a newly introduced time domain, termed natural time  $\chi$  (see below). It seems that this analysis enables the study of the dynamic evolution of a complex system and identifies when the system enters a critical stage. Natural time domain is optimal[58] for enhancing the signal’s localization in the time frequency space, which conforms to the desire to reduce uncertainty and extract signal information as much as possible. In a time series comprising  $N$  events, the *natural time*  $\chi_k = k/N$  serves as an index[40, 46, 47] for the occurrence of the  $k$ -th event. The evolution of the pair  $(\chi_k, Q_k)$  is studied[36, 40, 46, 47, 48, 49, 50, 51, 52, 53, 55, 56], where  $Q_k$  denotes a quantity proportional to the energy released in the  $k$ -th event. For example, for dichotomous signals, which is frequently the case of SES activities,  $Q_k$  stands for the duration of the  $k$ -th pulse. The normalized power spectrum  $\Pi(\omega) \equiv |\Phi(\omega)|^2$  was introduced[40, 46,

---

\*Electronic address: pvaro@otenet.gr

47], where

$$\Phi(\omega) = \sum_{k=1}^N p_k \exp\left(i\omega \frac{k}{N}\right) \quad (1)$$

and  $p_k = Q_k / \sum_{n=1}^N Q_n$ ,  $\omega = 2\pi\phi$ ;  $\phi$  stands for the *natural frequency*. The continuous function  $\Phi(\omega)$  should *not* be confused with the usual discrete Fourier transform, which considers only its values at  $\phi = 0, 1, 2, \dots$ . In natural time analysis[36, 40, 46, 47], the properties of  $\Pi(\omega)$  or  $\Pi(\phi)$  are studied for natural frequencies  $\phi$  less than 0.5, since in this range of  $\phi$ ,  $\Pi(\omega)$  or  $\Pi(\phi)$  reduces to a *characteristic function* for the probability distribution  $p_k$  in the context of probability theory. When the system enters the *critical* stage, the following relation holds[40, 46, 53]:

$$\Pi(\omega) = \frac{18}{5\omega^2} - \frac{6 \cos \omega}{5\omega^2} - \frac{12 \sin \omega}{5\omega^3}. \quad (2)$$

For  $\omega \rightarrow 0$ , Eq.(2) leads to[36, 40, 46]

$$\Pi(\omega) \approx 1 - 0.07\omega^2$$

which reflects[53] that the variance of  $\chi$  is given by

$$\kappa_1 = \langle \chi^2 \rangle - \langle \chi \rangle^2 = 0.07,$$

where  $\langle f(\chi) \rangle = \sum_{k=1}^N p_k f(\chi_k)$ . The entropy  $S$  in the natural time-domain is defined as[46, 49]

$$S \equiv \langle \chi \ln \chi \rangle - \langle \chi \rangle \ln \langle \chi \rangle,$$

which depends on the sequential order of events[50, 51]. It exhibits[52] concavity, positivity, Lesche[59, 60] stability, and for *infinitely* ranged temporal correlations its value is smaller[36, 49] than the value  $S_u (= \ln 2/2 - 1/4 \approx 0.0966)$  of a “uniform” (u) distribution (as defined in Refs. [46, 48, 49, 50, 51], e.g. when all  $p_k$  are equal or  $Q_k$  are positive independent and identically distributed random variables of finite variance. In this case,  $\kappa_1$  and  $S$  are designated  $\kappa_u (= 1/12)$  and  $S_u$ , respectively.) Thus,  $S < S_u$ . The same holds for the value of the entropy obtained[52, 55] upon considering the time reversal  $\mathcal{T}$ , i.e.,  $\mathcal{T}p_k = p_{N-k+1}$ , which is labelled by  $S_-$ . In summary, the SES activities, when analyzed in natural time exhibit *infinitely* ranged temporal correlations and obey the conditions[55, 56]:

$$\kappa_1 = 0.07 \quad (3)$$

and

$$S, S_- < S_u. \quad (4)$$

The scope of the present paper is twofold. First, a simple model is proposed (Section II) which, in the frame of natural time, leads to  $1/f^a$  behavior with an exponent  $a$  close to unity. The properties of this model in natural time are compared to those of the SES activities in Section III. This comparison is carried out by making use of the most recent experimental data of SES activities observed in Greece during the last several months. Section IV presents the conclusions.

TABLE I: The values of  $S$ ,  $\kappa_1$ ,  $S_-$  for the electric signals presented in Fig.5.

Date recorded	$S$	$\kappa_1$	$S_-$
Feb 8, 2007	0.067±0.007	0.074±0.007	0.079±0.007
Apr 23, 2007	0.071±0.005	0.069±0.003	0.066±0.005
Apr 24, 2007	0.072±0.003	0.067±0.003	0.069±0.003
Nov 7, 2007	0.070±0.005	0.065±0.005	0.070±0.005

## II. THE MODEL PROPOSED

### A. Description of the model

Here, we present a simple competitive evolution model which results, when analyzed in natural time, to  $1/f^a$  “noise” with  $a$  very close to unity. Let us consider the cardinality  $\epsilon_n$  of the family of sets  $S_n$  of successive extrema obtained from a given probability distribution function (PDF);  $S_0$  equals to the empty set. Each  $S_n$  is obtained by following the procedure described below for  $n$  times. Select a random number  $\eta_n$  from a given PDF and compare it with all the numbers of  $S_{n-1}$ . In order to construct the set  $S_n$ , we disregard from the set  $S_{n-1}$  all its members that are smaller than  $\eta_n$  and furthermore include  $\eta_n$ . Thus,  $S_n$  is a finite set of real numbers whose members are always larger or equal to  $\eta_n$ . Moreover  $\min[S_n] \geq \min[S_{n-1}]$  and  $\max[S_n] \geq \max[S_{n-1}]$ . The cardinality  $\epsilon_n \equiv |S_n|$  of these sets, which may be considered as equivalent to the dimensionality of the thresholds distribution in the coherent noise model (e.g. see Ref.[61] and references therein), if considered as time-series with respect to the natural number  $n$  (see Fig.1(a), which was drawn by means of the *exponential* PDF) exhibits  $1/f^a$  noise with  $a$  very close to unity, see Fig.1(b). This very simple model whose evolution is depicted in Fig.1(a), leads to a Detrended Fluctuation Analysis[9] (DFA) exponent  $\alpha_{DFA}$  close to unity, see Fig.1(c), being compatible with the  $1/f$  power spectrum depicted in Fig.1(b). The mathematical model described above corresponds to an asymptotically non-stationary process, since  $\langle \epsilon_n \rangle \propto \ln n$  with a variance  $\langle (\epsilon_n - \langle \epsilon_n \rangle)^2 \rangle \propto \ln n$  (see Fig.1(d)). Thus, in simple words, the present model suggests that the cardinality  $\epsilon_n$  of the family of sets  $S_n$  of successive extrema exhibits  $1/f^a$  behavior when considered as time-series with respect to the natural (time) number  $n$ . We note that a connection between  $1/f^a$  noise and extreme value statistics has been established and proposed as providing a new angle at the generic aspect of the phenomena[44]. Furthermore, in the frame of a formal similarity between the discrete spectrum of quantum systems and a discrete time series[14] the following striking similarity is noticed: The fact that  $a \approx 1$  together with the behavior  $\langle (\epsilon_n - \langle \epsilon_n \rangle)^2 \rangle \propto \ln n$  of the present model is reminiscent of the power law exponent and the  $\langle \delta_n^2 \rangle$  statistic in chaotic quantum systems[14, 15].

In order to check the stability of the results presented in Fig.1, we present in Fig.2(a) the average power spec-

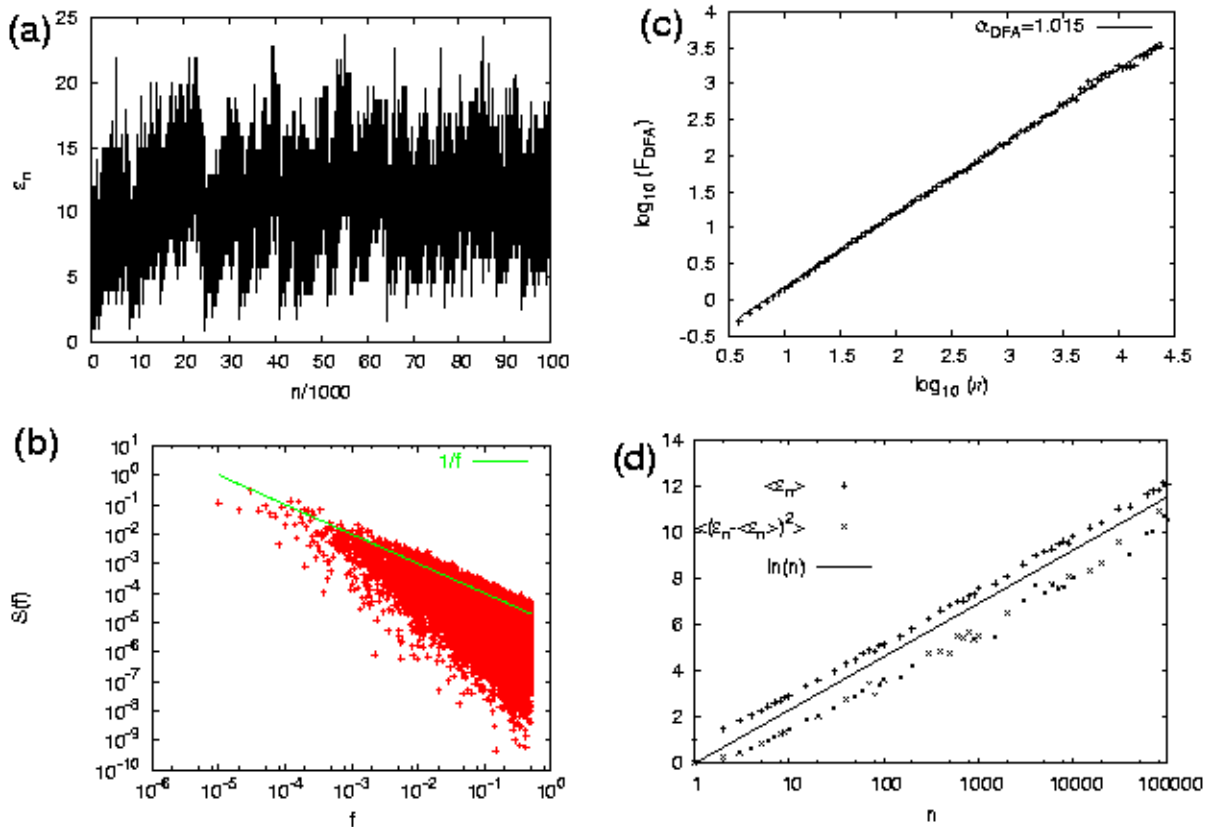


FIG. 1: (color online) (a): Example of the evolution of  $\epsilon_n$  (see the text) versus the number of renewals  $n$ , i.e., in natural time. (b): The Fourier power spectrum of (a); the (green) solid line corresponds to  $1/f$  and was drawn as a guide to the eye. (c): The DFA of (a) that exhibits an exponent  $\alpha_{DFA}$  very close to unity, as expected from (b). (d): Properties of the distribution of  $\epsilon_n$ . The average value  $\langle \epsilon_n \rangle$  (plus) and the variance  $\langle (\epsilon_n - \langle \epsilon_n \rangle)^2 \rangle$  (crosses) as a function of  $n$ . The straight solid line depicts  $\ln(n)$  and was drawn for the sake of reader's convenience.

trum obtained from  $10^4$  runs of the model. A sharp  $1/f$  behavior is observed. Moreover, in Fig.2(b), we present the results of the corresponding average values of  $F_{DFA-n}$  obtained from DFA of various orders  $n$  (i.e., when detrending with a polynomial of order  $n$ , see Ref.[62]). Figure 2(b) indicates that  $\alpha_{DFA-n}$  is close to unity.

## B. Analytical properties

We now discuss an analytical procedure which clarifies some properties of the model. In order to find analytically the distribution of the probabilities  $p(\epsilon_n)$ , one has simply to consider the possible outcomes when drawing  $n$  random numbers  $\eta_n$ . Since the selection is made by a means of a PDF, all these numbers are different from each other, thus -when sorted they- are equivalent to  $n$  points (sites) lying on the real axis. The value of  $\epsilon_n$  varies as  $\{\eta_n\}$  permute along these  $n$  sites *independently* from the PDF used in the calculation. Thus, a detailed study of the permutation group of  $n$  objects can lead to an exact solution of the model. It is well known, however, that

the number of the elements of this group is  $n!$  and this explains why we preferred to use the numerical calculation shown in Fig.1. Some exact results obtained by this method are the following:  $\langle \epsilon_1 \rangle = 1$ ;  $\langle \epsilon_2 \rangle = 1 + 1/2$ , since  $p(\epsilon_2 = 1) = p(\epsilon_2 = 2) = 1/2$ ;  $\langle \epsilon_3 \rangle = 1 + 1/2 + 1/3$ , since  $p(\epsilon_3 = 1) = 1/3$ ,  $p(\epsilon_3 = 2) = 1/2$  and  $p(\epsilon_3 = 3) = 1/6$ ;  $\langle \epsilon_4 \rangle = 1 + 1/2 + 1/3 + 1/4$  (see Fig.3). Figure 3 analyzes the results for  $n = 3$  (Fig.3(a)) and  $n = 4$  (Fig.3(b)). One can see that the probability  $p(\epsilon_n = m)$  equals to the sum of the  $n$  possible outcomes as  $\eta_n$  moves from the left to right in the  $n$  columns of Fig.3. In each column, the probability to have at the end  $\epsilon_n = m$  is just equal to the probability to keep  $m - 1$  numbers from the numbers already drawn that are larger than  $\eta_n$ . This results in

$$p(\epsilon_n = m) = \frac{1}{n} \sum_{k=m-1}^{n-1} p(\epsilon_k = m - 1) \quad (5)$$

(cf.  $p(\epsilon_0 = 0) = 1$ ).

Equation (5) enables us to calculate the characteristic

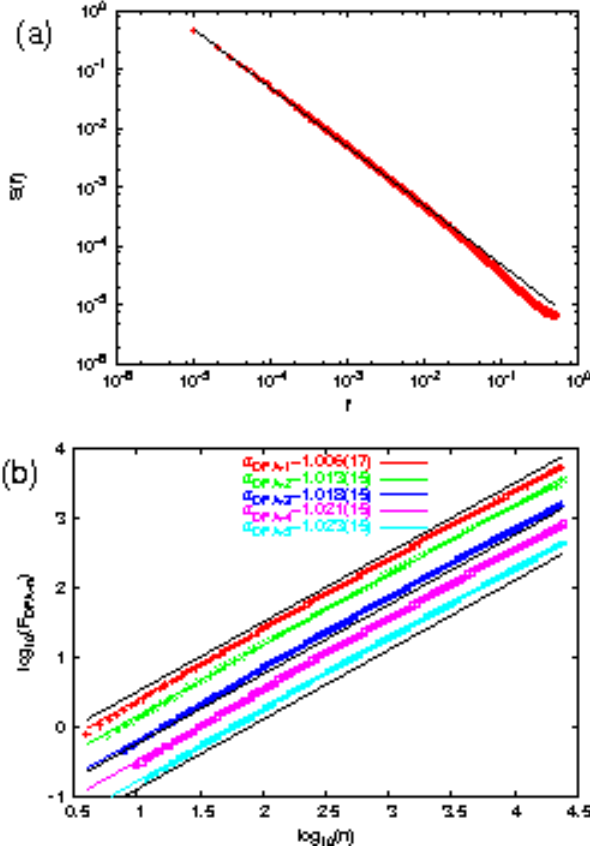


FIG. 2: (color online) Results from  $10^4$  runs of the model presented in Fig.1: (a) the average power spectrum, (b) Detrended Fluctuation Analyses of order  $n$  (DFA- $n$ )[62]. The black solid line in (a) corresponds to  $1/f$  spectrum and was drawn as a guide to the eye. For the same reason in (b), the black solid lines correspond to  $\alpha_{DFA} = 1$ . In (b), the colored solid lines correspond to the least square fit of the average  $F_{DFA-n}$ , depicted by symbols of the same color; the numbers in parentheses denote the standard deviation of  $\alpha_{DFA-n}$  obtained from the  $10^4$  runs of the model. The various  $F_{DFA-n}$  have been displaced vertically for the sake of clarity.

function (see p.928 of Ref.[63])

$$f_n(\lambda) \equiv \langle \exp(\lambda \epsilon_n) \rangle = \sum_{m=1}^n e^{\lambda m} p(\epsilon_n = m). \quad (6)$$

Indeed, by substituting  $p(\epsilon_n = m)$  in  $f_n(\lambda)$ , we obtain

$$n f_n(\lambda) = \sum_{m=1}^n e^{\lambda m} \sum_{k=m-1}^{n-1} p(\epsilon_k = m-1), \quad (7)$$

whereas by substituting  $p(\epsilon_{n+1} = m)$  in  $f_{n+1}(\lambda)$ , we find

$$(n+1) f_{n+1}(\lambda) = \sum_{m=1}^n e^{\lambda m} \sum_{k=m-1}^{n-1} p(\epsilon_k = m-1) + e^{\lambda} f_n(\lambda). \quad (8)$$

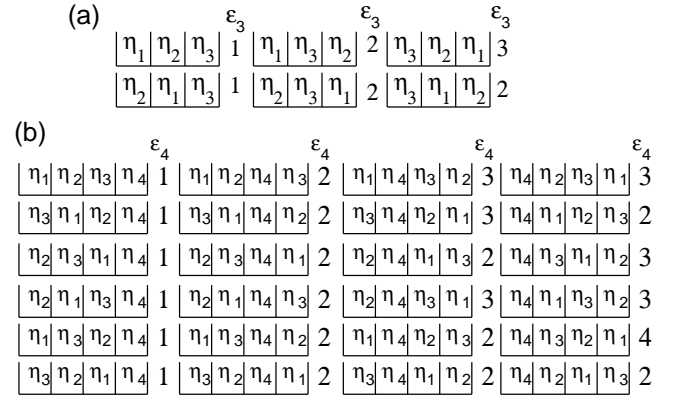


FIG. 3: The  $\eta_n$  values arranged in sites (bins) according to their value increasing from left to right. (a) The six ( $=3!$ ) equally probable outcomes after the selection of 3 random numbers by the same PDF. Actually, the sample space is (in one to one correspondence to) the permutations of 3 objects. (b) The 24 ( $=4!$ ) equally probable outcomes after the selection of 4 random numbers by the same PDF. Again, the sample space is (in one to one correspondence to) the permutations of 4 objects. For the reader's convenience, in each outcome, the corresponding  $\epsilon_n$ -value ( $n = 3$  or  $4$ ) is written. An inspection of (b), shows that  $p(\epsilon_4 = 1) = 1/4$ ,  $p(\epsilon_4 = 2) = 11/24$ ,  $p(\epsilon_4 = 3) = 1/4$  and  $p(\epsilon_4 = 4) = 1/24$ .

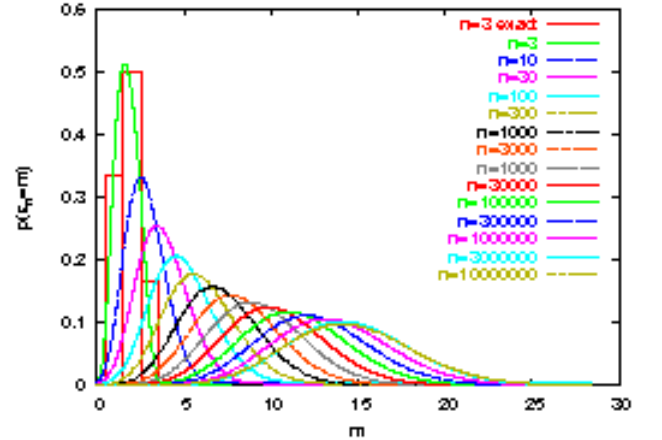


FIG. 4: (color online) The probabilities  $p(\epsilon_n = m)$  as a function of  $m$  for various  $n$ . The bar chart corresponds to the exact  $p(\epsilon_3 = m)$  whereas the continuous lines to the Cornish-Fisher approximation of Eq.(19). The latter approximation converges very rapidly to the true  $p(\epsilon_n = m)$ , see for example  $n = 3$ . This fact enables the calculation of  $p(\epsilon_n = m)$  for very large  $n$ , for which the recursive relation of Eq.(5) would accumulate significant round-off errors.

Subtracting now Eq.(7) from Eq.(8), we finally get

$$f_{n+1}(\lambda) = \frac{n + e^{\lambda}}{n + 1} f_n(\lambda). \quad (9)$$

Since  $f_1(\lambda) = e^{\lambda}$ , we find that Eq.(9) -upon considering

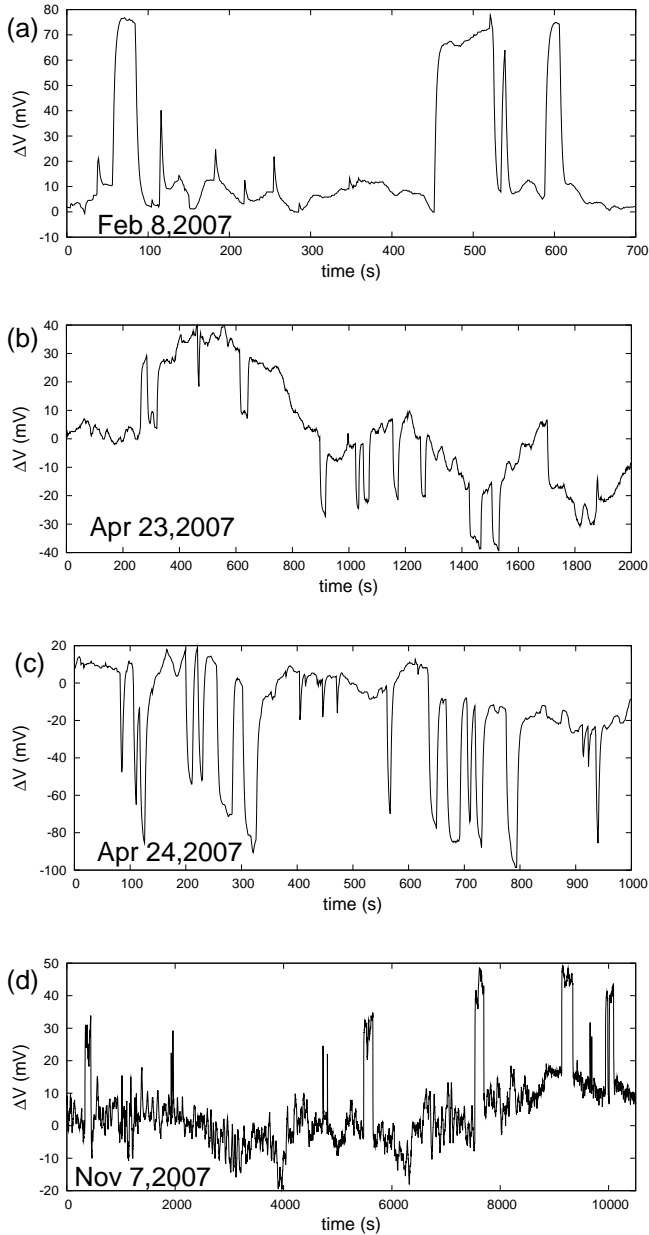


FIG. 5: Four electric signals recorded at PAT(sampling rate  $f_{exp}=1$  sample/sec) on February 8, 2007(a), April 23, 2007(b), April 24, 2007(c) and November 7, 2007(d).

Eq.6.1.22 of Ref.[63]- results in

$$f_n(\lambda) = \frac{1}{n!} \frac{\Gamma(e^\lambda + n)}{\Gamma(e^\lambda)}, \quad (10)$$

where  $\Gamma(x)$  is the gamma function. Now, the mean and all the central moments  $\mu_l \equiv \langle (\epsilon_n - \langle \epsilon_n \rangle)^l \rangle$  of the distribution of  $p(\epsilon_n = m)$  can be obtained by virtue of the

cumulant theorem (see p.928 of Ref.[63]):

$$\langle \epsilon_n \rangle = \left. \frac{d}{d\lambda} \ln f_n(\lambda) \right|_{\lambda=0}, \quad (11)$$

$$\mu_2 \equiv \langle (\epsilon_n - \langle \epsilon_n \rangle)^2 \rangle = \left. \frac{d^2}{d\lambda^2} \ln f_n(\lambda) \right|_{\lambda=0}, \quad (12)$$

$$\mu_3 \equiv \langle (\epsilon_n - \langle \epsilon_n \rangle)^3 \rangle = \left. \frac{d^3}{d\lambda^3} \ln f_n(\lambda) \right|_{\lambda=0}, \quad (13)$$

$$\mu_4 - 3\mu_2^2 = \left. \frac{d^4}{d\lambda^4} \ln f_n(\lambda) \right|_{\lambda=0}. \quad (14)$$

Substituting Eq.(10) into Eqs.(11) to (14) and using the properties of the polygamma functions (i.e., the n-th order logarithmic derivatives of the gamma function, see p.260 of Ref.[63]), we obtain

$$\langle \epsilon_n \rangle = \sum_{k=1}^n \frac{1}{k}, \quad (15)$$

$$\langle (\epsilon_n - \langle \epsilon_n \rangle)^2 \rangle = \sum_{k=1}^n \left( \frac{1}{k} - \frac{1}{k^2} \right), \quad (16)$$

$$\mu_3 = \sum_{k=1}^n \left( \frac{1}{k} - \frac{3}{k^2} + \frac{2}{k^3} \right), \quad (17)$$

$$\mu_4 - 3\mu_2^2 = \sum_{k=1}^n \left( \frac{1}{k} - \frac{7}{k^2} + \frac{12}{k^3} - \frac{6}{k^4} \right). \quad (18)$$

Equations (15) to (18) enable us to calculate the mean, standard deviation  $\sigma (= \sqrt{\mu_2})$ , skewness  $\gamma_1 = \mu_3/\sigma^3$  and kurtosis  $\gamma_2 = \mu_4/\sigma^4 - 3$  as a function of  $n$ . Using now the Cornish-Fisher (CF) expansion treated in Ref.[64], we obtain the following continuous approximation to  $p(\epsilon_n = m)$

$$p_{CF}(\tilde{\epsilon}_n) = \frac{1}{\sqrt{2\pi}} \left| 1 - \frac{\gamma_1}{3} \tilde{\epsilon}_n + \frac{\gamma_1^2}{36} (12\tilde{\epsilon}_n^2 - 7) - \frac{\gamma_2}{8} (\tilde{\epsilon}_n^2 - 1) \right| \times \exp \left\{ -\frac{1}{2} \left[ \tilde{\epsilon}_n - \frac{\gamma_1}{6} (\tilde{\epsilon}_n^2 - 1) - \frac{\gamma_2}{24} (\tilde{\epsilon}_n^3 - 3\tilde{\epsilon}_n) + \frac{\gamma_1^2}{36} (4\tilde{\epsilon}_n^3 - 7\tilde{\epsilon}_n) \right]^2 \right\}$$

where  $\tilde{\epsilon}_n = (\epsilon_n - \langle \epsilon_n \rangle)/\sigma$ . Equation (19), although being a continuous approximation to the point probabilities  $p(\epsilon_n = m)$ , rapidly converges to the latter, see for example the comparison of the exact  $p(\epsilon_3 = m)$  and the corresponding  $p_{CF}(\tilde{\epsilon}_3)/\sigma$  in Fig.4. An inspection of this figure, which depicts the probabilities  $p(\epsilon_n = m)$  up to  $n = 10^7$ , reveals that even for large  $n$ , the probability  $p(\epsilon_n = m)$  remains non-Gaussian (cf. even at  $n = 10^9$ , we obtain from Eqs.(16) to (18)  $\gamma_1 = 0.2154 \neq 0$  with  $\gamma_2 = 0.0459 \neq 0$ ).

### III. COMPARISON OF THE MODEL WITH THE SES PHYSICAL PROPERTIES IN NATURAL TIME

We first present in III A the most recent experimental results on Seismic Electric Signals and then compare in

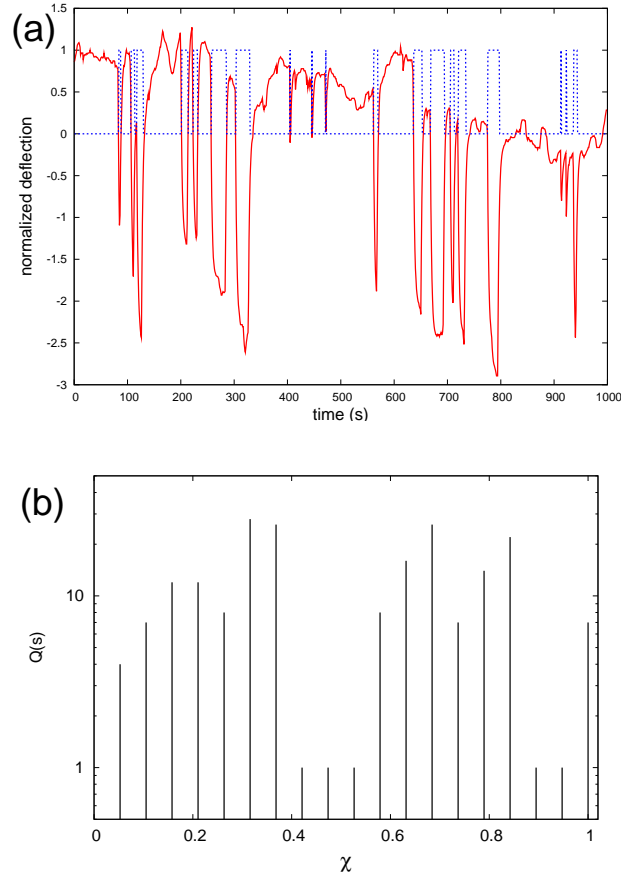


FIG. 6: (color online) (a): The electric signal depicted in Fig.5(c) (April 24,2007) in normalized units (i.e., by subtracting the mean value and dividing the results by the standard deviation) along with its dichotomous representation which is marked by the dotted (blue) line. (b): How the signal in (a) is read in natural time.

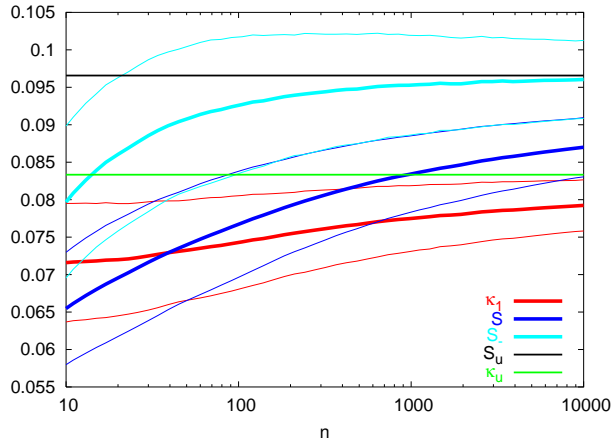


FIG. 7: (color online) Evolution of the parameters of  $\kappa_1$ ,  $S$  and  $S_-$  as a function of  $n$ , when  $\epsilon_n$  are analyzed in the natural time domain. The thick lines correspond to the average value of  $\kappa_1$ ,  $S$  and  $S_-$ , found by  $10^4$  runs of the model. The thinner lines correspond to the  $\pm$ one standard deviation confidence intervals. For the reader's convenience, the green and black horizontal lines show the values  $\kappa_u$  and  $S_u$  of  $\kappa_1$  and  $S$ , respectively, that correspond to a “uniform” distribution.

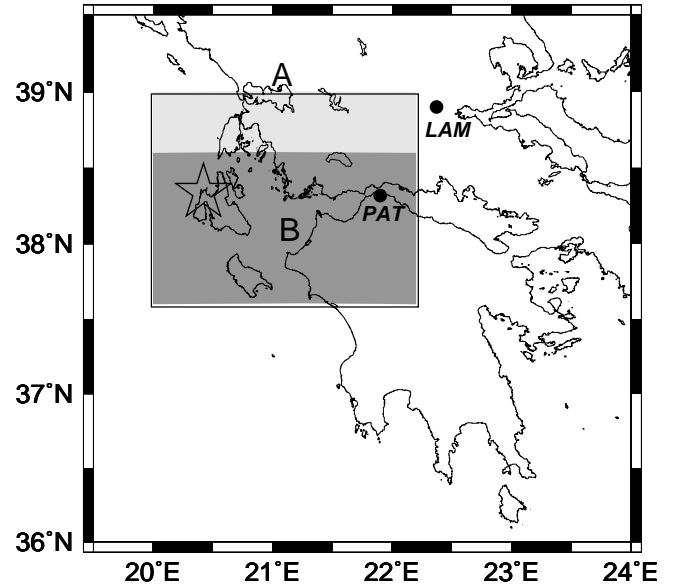


FIG. 8: The map shows the areas A,B. The star indicates the epicenter of the strong 6.0 EQ that occurred on March 25, 2007 in Kefallonia.

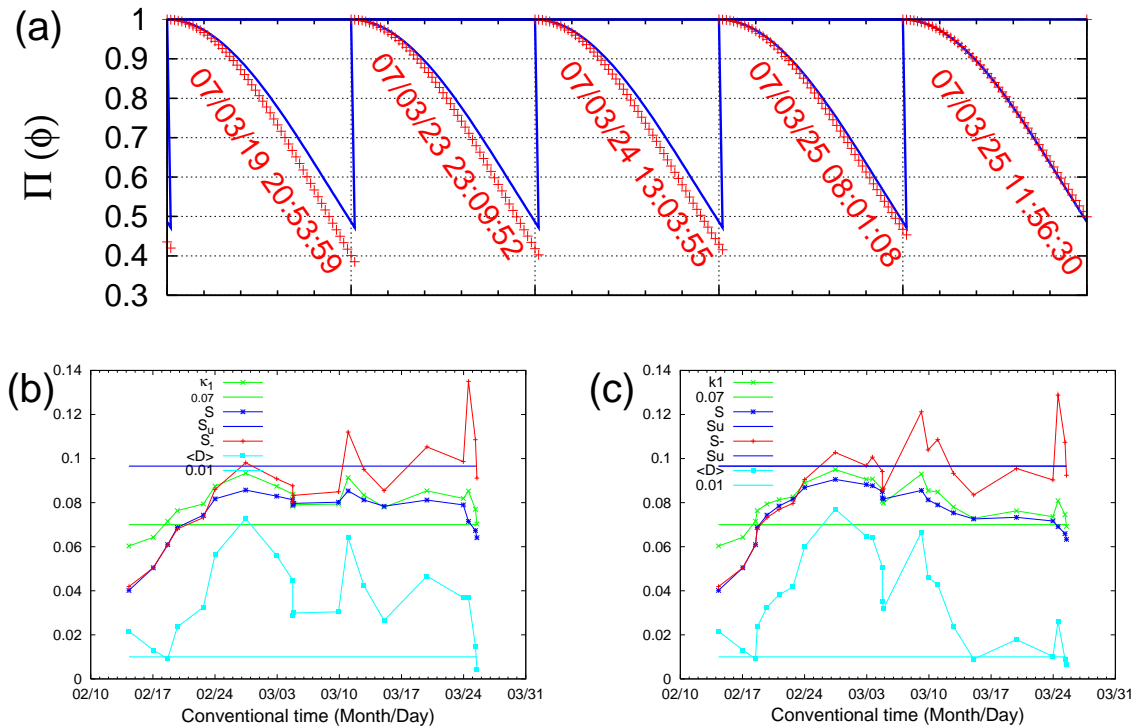


FIG. 9: (color online) (a) The normalized power spectrum (red)  $\Pi(\phi)$  of the seismicity as it evolves event by event (whose date and time (UT) of occurrence are written in each panel) after the initiation of the SES activity on February 8, 2007. The excerpt presented here refers to the period 19 to 25 March, 2007 and corresponds to the area B,  $M_{thres} = 3.2$ . In each case only the spectrum in the area  $\phi \in [0, 0.5]$  is depicted (separated by the vertical dotted lines), whereas the  $\Pi(\phi)$  of Eq.(2) is depicted by blue color. The minor horizontal ticks for  $\phi$  are marked every 0.1. (b), (c) Evolution of the parameters ( $D$ ),  $\kappa_1$ ,  $S$  and  $S_-$  after the initiation of the SES activity on February 8, 2007 for the areas B ( $M_{thres} = 3.2$ ) and A ( $M_{thres} = 3.2$ ), respectively, until just before the 6.0 EQ.

III B their properties with the results of the model proposed.

#### A. The recent electric field data

Figure 5 depicts the original time series of four electrical disturbances that have been recently recorded on: (a) February 8, 2007, (b) April 23, 2007, (c) April 24, 2007 and (d) November 7, 2007 at a measuring station termed Patras (PAT) located at  $\approx 160$ km west of Athens. All these four recent signals were analyzed in natural time. For example, if we read in natural time the signal on April 24, 2007 (Fig.5(c)) -the dichotomous representation of which is marked by the dotted (blue) line in Fig.6(a)-we find the natural time representation of Fig.6(b) the analysis of which leads to the values  $\kappa_1 = 0.067 \pm 0.003$ ,  $S = 0.072 \pm 0.003$ ,  $S_- = 0.069 \pm 0.003$ . The relevant results of all the four signals are compiled in Table I and found to be consistent with the conditions (3) and (4), thus they can be classified as SES activities (for their subsequent seismicity see the Appendix). An inspection of Table I shows that the  $S$  value is more or less comparable to that of  $S_-$ , but experimental uncertainty does not allow any conclusion which of them is larger. Note

that in several former examples[52], the data analysis also showed that the  $S$  value may either be smaller or larger than  $S_-$ .

#### B. Comparison of the SES properties with those of the model proposed

We now turn to investigate whether the parameters  $\kappa_1$ ,  $S$  and  $S_-$  deduced from the  $1/f$  model of Section II are consistent to those resulted from the analysis of the SES activities observed. Figure 7 summarizes the results of  $10^4$  runs of the model which, for moderate sizes of  $n$ , seems to obey more or less the conditions (3) and (4). In particular, for  $n \lesssim 10^2$  (which is frequently the number of pulses of the SES activities observed in field experiments), Fig.7 shows that  $\kappa_1$  is close to 0.070,  $S < S_u$  and (in most cases)  $S_- < S_u$ . A closer inspection of Fig.7, however, reveals the following incompatibility of the model with the experimental results: For  $n \lesssim 10^2$ , the model clearly suggests that  $S_- > S$ , thus disagreeing with the experimental data which show, as mentioned above, that  $S$  may either be smaller or larger than  $S_-$ . The origin of this incompatibility has not been fully understood. It might be due to the fact that SES activities

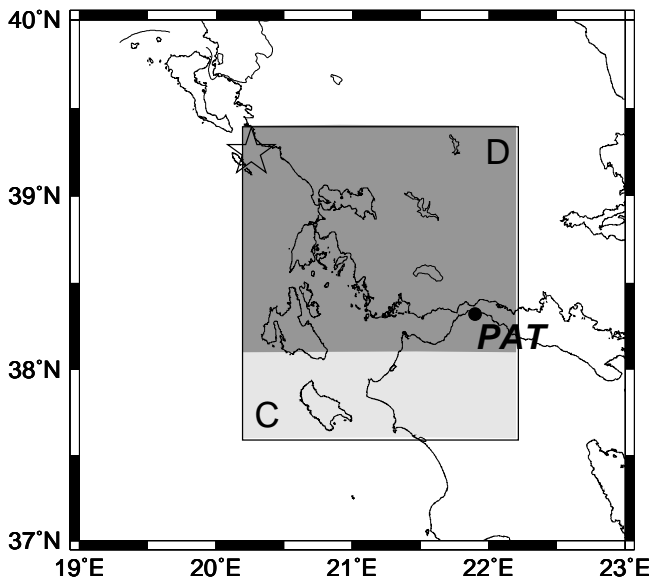


FIG. 10: The map shows the areas C and D. The star shows the epicenter of the strong 5.8 EQ at 18:09:11 on June 29, 2007.

exhibit *critical* dynamics, while the model cannot capture all the characteristics of such dynamics.

#### IV. CONCLUSIONS

In summary, using the newly introduced concept of natural time: (a) A simple model is proposed that exhibits  $1/f^a$  behavior with  $a$  close to unity. (b) Electric signals, recorded during the last few months in Greece, are classified as SES activities since they exhibit *infinitely* ranged temporal correlations. Actually, two magnitude 6.0 class earthquakes already occurred in western Greece (see the Appendix). (c) For sizes  $n$  comparable to those of the SES activities measured in the field experiments (i.e.,  $n \lesssim 10^2$ ), the model proposed here leads to values of the parameters  $\kappa_1$  ( $\approx 0.070$ ) and  $S, S_-$  ( $< S_u$ ) that are consistent with those deduced from the SES activities analysis. Despite of this fact, however, the model results in  $S_-$  values that are almost always larger than those of  $S$ , while the observed SES activities result in  $S$  values that may either be larger or smaller than  $S_-$ . This discrepancy might be due to the inability of the model to capture the characteristics of *critical* dynamics which is exhibited by SES activities.

#### APPENDIX: WHAT HAPPENED AFTER THE SES ACTIVITIES DEPICTED IN FIG.5

We clarify that, during the last decade, preseismic information[65] based on SES activities is issued *only* when the magnitude of the strongest EQ of the impending EQ activity is estimated -by means of the SES

amplitude[26, 27, 28, 29, 30] to be comparable to 6.0 units or larger[36]. Here, we explain what happened after the SES activity at PAT on February 8, 2007 (see Fig.5(a)) and on April 23 and 24, 2007 (see Figs.5(b),(c)). The analysis concerning the most recent activity on November 7, 2007, is still in progress.

#### 1. What happened after the SES activity of February 8, 2007

According to the Athens observatory (the seismic data of which will be used here), a strong earthquake (EQ) with magnitude 6.0-units occurred at Kefallonia area, i.e., 38.34°N 20.42°E, at 13:57 UT on March 25, 2007. We show below that the occurrence time of this strong EQ can be estimated by following the procedure described in Refs.[36, 46, 53, 55, 56].

We study how the seismicity evolved after the recording of the SES activity at PAT on February 8, 2007, by considering either the area A:  $N_{37.6}^{39.0} E_{20.0}^{22.2}$  or its smaller area B:  $N_{37.6}^{38.6} E_{20.0}^{22.2}$  (see Fig.8). If we set the natural time for seismicity zero at the initiation of the SES activity on February 8, 2007, we form time series of seismic events in natural time for various time windows as the number  $N$  of consecutive (small) EQs increases. We then compute the normalized power spectrum in natural time  $\Pi(\phi)$  for each of the time windows. Excerpt of these results, which refers to the values deduced during the period from 20:53:59 UT on March 19, 2007, to 11:56:30 UT on 25 March, 2007, is depicted in red in Fig.9(a). This figure corresponds to the area B with magnitude threshold (hereafter referring to the local magnitude ML or the ‘duration’ magnitude MD)  $M_{thres} = 3.2$ . In the same figure, we plot in blue the power spectrum obeying the relation (2) which holds, as mentioned, when the system enters the *critical* stage. The date and the time of the occurrence of each small earthquake (with magnitude exceeding (or equal to) the aforementioned threshold) that occurred in area B, is also written in red in each panel. An inspection of this figure reveals that the red line approaches the blue line as  $N$  increases and a *coincidence* occurs at the last small event which had a magnitude 3.2 and occurred at 11:56:30 UT on March 25, 2007, i.e., just two hours before the strong 6.0 EQ. To ensure that this coincidence is a *true* one (see also below) we also calculate the evolution of the quantities  $\kappa_1, S$  and  $S_-$  and the results are depicted in Fig. 9(b) and 9(c) for the same magnitude thresholds for each of the areas B and A, respectively.

The conditions for a coincidence to be considered as *true* are the following (e.g., see Refs.[36, 46, 53, 55, 56]): First, the ‘average’ distance  $\langle D \rangle$  between the empirical and the theoretical  $\Pi(\phi)$  (i.e., the red and the blue line, respectively, in Fig.9(a)) should be smaller than  $10^{-2}$ . See Fig. 9(b),(c) where we plot  $\langle D \rangle$  versus the conventional time for the aforementioned two areas B and A, respectively. Second, in the examples observed to date,

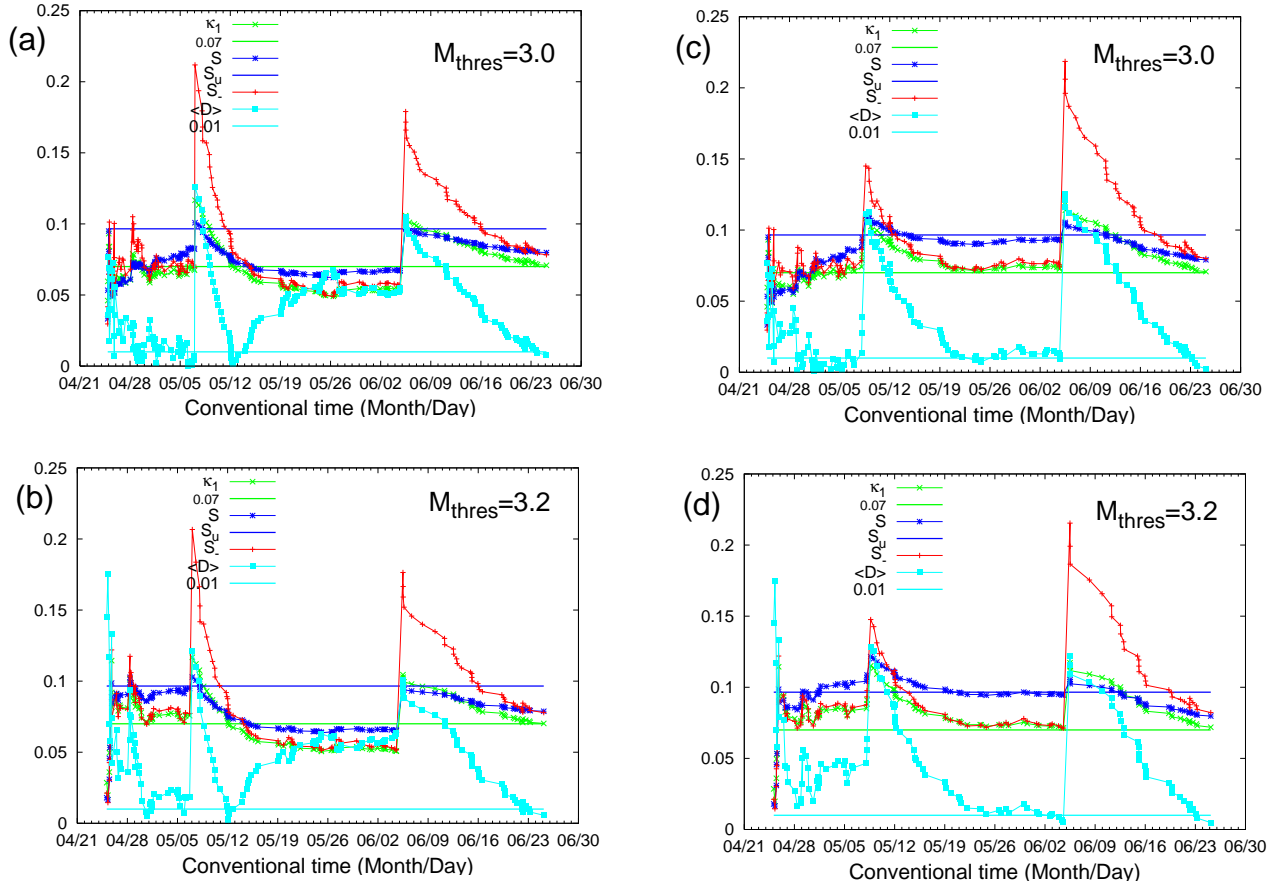


FIG. 11: (color online) (a),(b) and (c),(d) depict the evolution of the parameters  $\langle D \rangle$ ,  $\kappa_1$ ,  $S$  and  $S_-$  after the initiation of the SES activity on April 24, 2007 for the areas C and D, respectively (for two magnitude thresholds in each area), until 03:40:15 UT on June 25, 2007.

a few events *before* the coincidence leading to the strong EQ, the evolving  $\Pi(\phi)$  has been found to approach that of the relation (2), i.e., the blue one in Fig.9(a), from *below* (cf. this reflects that during this approach the  $\kappa_1$ -value decreases as the number of events increases). In addition, both values  $S$  and  $S_-$  should be smaller than  $S_u$  at the coincidence. Finally, since the process concerned is self-similar (*critical* dynamics), the time of the occurrence of the (true) coincidence should *not* change, in principle, upon changing the surrounding area (and the magnitude threshold  $M_{thres}$ ) used in the calculation. Note that in Fig. 9(b), upon the occurrence of the aforementioned last small event at 11:56:30 UT of March 25, 2007, in area B the  $\langle D \rangle$  value becomes smaller than  $10^{-2}$ . The same was found to hold for the area A, see Fig.9(c).

## 2. What happened after the SES activities of April 23 and 24, 2007

We investigate the seismicity after the aforementioned SES activities depicted in Figs.5(b) and 5(c). The in-

vestigation is made in the areas C:  $N_{37.6}^{39.4} E_{20.2}^{22.2}$  and D:  $N_{38.1}^{39.4} E_{20.2}^{22.2}$  (see Fig.10). Starting the computation of seismicity from the initiation of the SES activity on April 24, 2007 (which, between the two SES activities depicted in Figs.5(b) and 5(c), has the higher actual amplitude), we obtain the results depicted in Figs.11(a),(b) and 11(c),(d) for the areas C and D, respectively, for  $M_{thres} = 3.0$  and  $M_{thres} = 3.2$ . An inspection of the parameters  $\langle D \rangle$ ,  $\kappa_1$ ,  $S$  and  $S_-$  reveals that they exhibited a *true* coincidence (as discussed above) around June 25, 2007, i.e., around four days before the 5.8 EQ that occurred at 18:09:11 UT on June 29, 2007, with an epicenter at  $39.3^\circ N$   $20.3^\circ E$  (shown by a star in Fig.10).

## 3. Study of the seismicity after the SES activity on November 7, 2007

This study (along the lines explained above) is still in progress by investigating the seismicity in the area B of Fig.8 as well as in the larger area, i.e.,  $N_{37.6}^{38.6} E_{23.3}^{20.0}$ .

- 
- [1] B. B. Mandelbrot, *Multifractals and 1/f Noise* (Springer-Verlag, New York, 1999).
- [2] T. Antal, M. Droz, G. Györgyi, and Z. Rácz, *Phys. Rev. E* **65**, 046140 (2002).
- [3] M. B. Weissman, *Rev. Mod. Phys.* **60**, 537 (1988).
- [4] T. Musha and H. Higuchi, *Jpn. J. Appl. Phys.* **15**, 1271 (1976).
- [5] K. Nagel and M. Paczuski, *Phys. Rev. E* **51**, 2909 (1995).
- [6] X. Zhang and G. Hu, *Phys. Rev. E* **52**, 4664 (1995).
- [7] A. Nakahara and T. Isoda, *Phys. Rev. E* **55**, 4264 (1997).
- [8] A. L. Goldberger, L. A. N. Amaral, J. M. Hausdorff, P. C. Ivanov, C.-K. Peng, and H. E. Stanley, *Proc. Natl. Acad. Sci. USA* **99**, 2466 (2002).
- [9] C.-K. Peng, J. Mietus, J. M. Hausdorff, S. Havlin, H. E. Stanley, and A. L. Goldberger, *Phys. Rev. Lett.* **70**, 1343 (1993).
- [10] S. Mercik, K. Weron, and Z. Ziwy, *Phys. Rev. E* **60**, 7343 (1999).
- [11] B. Mandelbrot and J. R. Wallis, *Water Resour. Res.* **5**, 321 (1969).
- [12] F. Lillo and R. N. Mantegna, *Phys. Rev. E* **62**, 6126 (2000).
- [13] J. M. G. Cómez, A. Relaño, J. Retamosa, E. Faleiro, L. Salasnich, M. Vraničar, and M. Robnik, *Phys. Rev. Lett* **94**, 084101 (2005).
- [14] A. Relaño, J. M. G. Cómez, R. A. Molina, J. Retamosa, and E. Faleiro, *Phys. Rev. Lett* **89**, 244102 (2002).
- [15] M. S. Santhanam and J. N. Bandyopadhyay, *Phys. Rev. Lett.* **95**, 114101 (2005).
- [16] M. S. Santhanam, J. N. Bandyopadhyay, and D. Angom, *Phys. Rev. E* **73**, 015201 (2006).
- [17] W. H. Press, *Comments Astrophys.* **7**, 103 (1978).
- [18] D. L. Gilder, T. Thornton, and M. W. Mallon, *Science* **267**, 1837 (1995).
- [19] H. Yoshinaga, S. Miyazima, and S. Mitake, *Physica A* **280**, 582 (2000).
- [20] J. M. Berger and B. B. Mandelbrot, *IBM J. Res. Dev.* **7**, 224 (1963).
- [21] S. Kogan, *Electronic Noise and Fluctuations in Solids* (Cambridge University Press, Cambridge, 1996).
- [22] P. G. Collins, M. S. Fuhrer, and A. Zettl, *Appl. Phys. Lett.* **76**, 894 (2000).
- [23] L. B. Kiss, U. Klein, C. M. Muirhead, J. Smithyman, and Z. Gingl, *Solid State Commun.* **101**, 51 (1997).
- [24] D. Sornette, *Critical Phenomena in the Natural Sciences: Chaos, Fractals, Selforganization, and Disorder: Concepts and Tools* (Springer-Verlag, Berlin, 2000).
- [25] A. V. Yakimov and F. N. Hooge, *Physica B-condensed matter* **291**, 97 (2000).
- [26] P. Varotsos and K. Alexopoulos, *Tectonophysics* **110**, 73 (1984).
- [27] P. Varotsos, K. Alexopoulos, K. Nomicos, and M. Lazaridou, *Nature (London)* **322**, 120 (1986).
- [28] P. Varotsos, K. Alexopoulos, K. Nomicos, and M. Lazaridou, *Tectonophysics* **152**, 193 (1988).
- [29] P. Varotsos and M. Lazaridou, *Tectonophysics* **188**, 321 (1991).
- [30] P. Varotsos, K. Alexopoulos, and M. Lazaridou, *Tectonophysics* **224**, 1 (1993).
- [31] P. V. Varotsos, N. V. Sarlis, and M. S. Lazaridou, *Phys. Rev. B* **59**, 24 (1999).
- [32] N. Sarlis, M. Lazaridou, P. Kapisir, and P. Varotsos, *Geophys. Res. Lett.* **26**, 3245 (1999).
- [33] P. Varotsos, N. Sarlis, and M. Lazaridou, *Acta Geophys. Pol.* **48**, 141 (2000).
- [34] P. Varotsos, N. Sarlis, and E. Skordas, *Acta Geophys. Pol.* **48**, 263 (2000).
- [35] P. Varotsos and K. Alexopoulos, *Thermodynamics of Point Defects and their Relation with Bulk Properties* (North Holland, Amsterdam, 1986).
- [36] P. Varotsos, *The Physics of Seismic Electric Signals* (TERRAPUB, Tokyo, 2005).
- [37] P. Varotsos, N. Sarlis, and E. Skordas, *Proc. Jpn. Acad., Ser. B: Phys. Biol. Sci.* **77**, 87 (2001).
- [38] P. Varotsos, N. Sarlis, and E. Skordas, *Proc. Jpn. Acad., Ser. B: Phys. Biol. Sci.* **77**, 93 (2001).
- [39] P. A. Varotsos, N. V. Sarlis, and E. S. Skordas, *Phys. Rev. Lett.* **91**, 148501 (2003).
- [40] P. A. Varotsos, N. V. Sarlis, and E. S. Skordas, *Phys. Rev. E* **66**, 011902 (2002).
- [41] A. Weron, K. Burnecki, S. Mercik, and K. Weron, *Phys. Rev. E* **71**, 016113 (2005).
- [42] P. Bak, C. Tang, and K. Wiesenfeld, *Phys. Rev. Lett.* **59**, 381 (1987).
- [43] P. Bak, *How Nature Works* (Copernicus, New York, 1996).
- [44] T. Antal, M. Droz, G. Györgyi, and Z. Rácz, *Phys. Rev. Lett* **87**, 240601 (2001).
- [45] J. Davidsen and H. G. Schuster, *Phys. Rev. E* **65**, 026120 (2002).
- [46] P. A. Varotsos, N. V. Sarlis, and E. S. Skordas, *Practica of Athens Academy* **76**, 294 (2001).
- [47] P. A. Varotsos, N. V. Sarlis, and E. S. Skordas, *Acta Geophys. Pol.* **50**, 337 (2002).
- [48] P. A. Varotsos, N. V. Sarlis, and E. S. Skordas, *Phys. Rev. E* **67**, 021109 (2003).
- [49] P. A. Varotsos, N. V. Sarlis, and E. S. Skordas, *Phys. Rev. E* **68**, 031106 (2003).
- [50] P. A. Varotsos, N. V. Sarlis, E. S. Skordas, and M. S. Lazaridou, *Phys. Rev. E* **70**, 011106 (2004).
- [51] P. A. Varotsos, N. V. Sarlis, E. S. Skordas, and M. S. Lazaridou, *Phys. Rev. E* **71**, 011110 (2005).
- [52] P. A. Varotsos, N. V. Sarlis, H. K. Tanaka, and E. S. Skordas, *Phys. Rev. E* **71**, 032102 (2005).
- [53] P. A. Varotsos, N. V. Sarlis, H. K. Tanaka, and E. S. Skordas, *Phys. Rev. E* **72**, 041103 (2005).
- [54] N. V. Sarlis, P. A. Varotsos, and E. S. Skordas, *Phys. Rev. B* **73**, 054504 (2006).
- [55] P. A. Varotsos, N. V. Sarlis, E. S. Skordas, H. K. Tanaka, and M. S. Lazaridou, *Phys. Rev. E* **73**, 031114 (2006).
- [56] P. A. Varotsos, N. V. Sarlis, E. S. Skordas, H. K. Tanaka, and M. S. Lazaridou, *Phys. Rev. E* **74**, 021123 (2006).
- [57] P. A. Varotsos, N. V. Sarlis, E. S. Skordas, and M. S. Lazaridou, *Appl. Phys. Lett.* **91**, 064106 (2007).
- [58] S. Abe, N. V. Sarlis, E. S. Skordas, H. K. Tanaka, and P. A. Varotsos, *Phys. Rev. Lett.* **94**, 170601 (2005).
- [59] B. Lesche, *J. Stat. Phys.* **27**, 419 (1982).
- [60] B. Lesche, *Phys. Rev. E* **70**, 017102 (2004).
- [61] U. Tirnakli and S. Abe, *Phys. Rev. E* **70**, 056120 (2004).
- [62] K. Hu, P. C. Ivanov, Z. Chen, P. Carpena, and H. E. Stanley, *Phys. Rev. E* **64**, 011114 (2001).
- [63] M. Abramowitz and I. Stegun, *Handbook of Mathematical*

*Functions* (Dover, New York, 1970).

[64] V. K. B. Kota, V. Potbhare, and P. Shenoy, *Phys. Rev. C* **34**, 2330 (1986).

[65] P. A. Varotsos, N. V. Sarlis, and E. S. Skordas (2007), [cond-mat/0703683](https://arxiv.org/abs/cond-mat/0703683).